Effect of icosahedral and cuboctahedral symmetries on the electronic and magnetic structure of $MnAl_n$

V. de Coulon
Institut Roman de Recherche Numérique en Physique des Matériaux, Ecole Polytechnique Fédérale de Lausanne, CH-1015 Lausanne, Switzerland

F. A. Reuse
Institut de Physique Expérimentale, Ecole Polytechnique Fédérale de Lausanne, CH-1015 Laussane, Switzerland

S. N. Khanna
Physics Department, Virginia Commonwealth University, Richmond, Virginia 23284-2000
(Received 21 September 1992; revised manuscript received 8 March 1993)

The effect of local symmetry on the magnetic moment at the Mn sites in Mn_xAl_{1-x} quasicrystals has been investigated by modeling the quasicrystals by clusters. Our studies based on the self-consistent density-functional calculations on clusters having a central Mn surrounded by Al_n ($n \leq 54$) atoms in cuboctahedral and icosahedral arrangement show that the Mn sites do carry a moment at small cluster sizes. The moment is, however, quenched as the cluster size is increased irrespective of the geometry. This quenching is shown to be a direct consequence of the mixing between the Mn d states and the Al p states in these geometries. The existing theoretical picture, which is based on calculations on smaller clusters and predicts that the magnetic Mn sites in MnAl quasicrystals are a result of icosahedral symmetry, is shown to be incorrect.

I. INTRODUCTION

Ever since the report of long-range icosahedral symmetry in rapidly solidified $Mn_{14}Al_{86}$ by Shechtman and coworkers,[1] quasicrystalline (QC) materials have attracted theoretical and experimental interest. As is well known, these materials exhibit the local icosahedral symmetry absent in conventional periodic solids. One of the basic issues has been the effect of this symmetry on the magnetic properties. For example, experimental investigations involving magnetic susceptibility by NMR and other measurements[2] on Mn_xAl_{1-x} QC show that a large fraction of Mn sites in these QC's possesses a paramagnetic moment ranging from 0.5 to $1.5\mu_B$ for Mn content ranging from 14 to 22 %. It is also found that the Mn sites in $MnAl_6$ orthorhombic crystals having the same Mn content do not carry any magnetic moment.[3] Various geometrical models[4] as well as models based on experimental diffraction data[5] show that the Mn atoms in MnAl materials occupy sites of various local symmetries with a substantial fraction occupying centers of Mackay icosahedron.[6] The fact that the Mn sites in ordered $Mn_{14}Al_{86}$ are nonmagnetic whereas the QC system containing the same Mn concentration shows Mn sites with a distribution of moments[7] raises the question whether the magnetic moments on Mn sites are stabilized by the icosahedral local symmetry. This is particularly interesting since a different picture emerges if one considers the moment on Mn sites as a function of Mn concentration. It is found that the MnAl QC alloys with Mn concentration less than 5% are nonmagnetic.[8] As the Mn concentration is increased beyond 5%, the alloys become magnetic and the effective moment on Mn sites increases as the square of the Mn concentration. These results show that Mn-Mn interactions probably play a role in stabilizing the Mn moment.

To understand the experimental findings, two theoretical calculations modeling quasicrystals by small finite clusters have been carried out. McHenry *et al.*[9] used a multiple-scattering X-α (MS-X-α) technique to study a $MnAl_{32}$ atom icosahedral cluster and a $MnAl_{18}$ cuboctahedral cluster. Bagayoko *et al.*[10] also carried out density-functional calculations on a $MnAl_{18}$ cluster. It was found that while the Mn site did not carry a moment in cuboctahedral cluster, the Mn site had a moment of $3.6\mu_B$ in icosahedral cluster. This has been taken to imply that the icosahedral symmetry is responsible for the formation of magnetic Mn sites in MnAl QC's. Note that the concentration of Mn in $MnAl_{32}$ is around 3% and according to experiment,[8] the QC alloy is nonmagnetic at this concentration. One is then left to wonder if the finite moment in theory is an artifact of the small cluster used to mimic the solid and if the conclusions would change if bigger clusters were used.

The purpose of this paper is to focus on the relation between the symmetry and the magnetic moment on a Mn site. The basic issue we want to address is whether the icosahedral symmetry alone is sufficient to stabilize the moment at the Mn sites.

Our studies are based on *ab initio* density-functional calculations and are carried out on icosahedral and cuboctahedral clusters containing a central Mn atom surrounded by up to 54 Al atoms. We show that the Mn sites are magnetic for small cluster sizes in accordance

0163-1829/93/48(2)/814(15)/$06.00

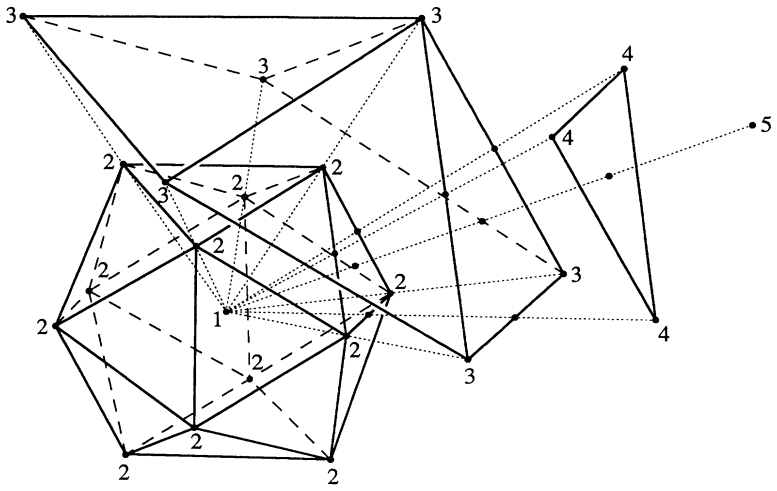

FIG. 1. Geometrical structure of the Al shells (orbits) in the icosahedral symmetry of $MnAl_n$. O_1 is the central Mn site labeled by 1. O_2 forms an icosahedron of 12 Al sites labeled by 2. O_3 is also an icosahedron of 12 Al sites labeled by 3 (only 6 sites have been represented in this figure). O_4 is formed by 30 middle points of the edge of an icosahedron labeled by 4 (only 3 sites are shown). Finally, O_5 is a dodecahedron formed by 20 central points of the faces of an icosahedron labeled by 5 (only 1 site has been shown).

with previous studies. However, the moment disappears as the cluster size is increased. Since an individual Mn atom has a spin moment of $5.0\mu_B$, we carry out a detailed investigation of the electronic coupling between the s, p, and d states in Mn and the s and p states in Al and we show how this hybridization depends on cluster size and geometry and quenches the Mn moment at large sizes.

In Sec. II, we briefly summarize the size and symmetry of the clusters studied in the present work and in Sec. III we discuss the theoretical techniques used by us. Section IV contains our investigations on icosahedral clusters and Sec. V contains our results on cuboctahedral clusters. Finally, Sec. VI is devoted to conclusions.

II. SYMMETRY AND SIZE OF MODEL CLUSTERS

To facilitate the presentation and discussion of our results and to familiarize the reader with our notations, we briefly discuss the geometry and the symmetry groups I_h and O_h associated with the icosahedral and cuboctahedral geometries. The point group I_h contains 120 elements; it is formed by 60 rotations plus 60 pseudorotations including the space reflection. The cubic point group O_h contains 48 elements; it is formed by 24 rotations plus 24 pseudorotations including the space reflection.

In Figs. 1 and 2, we show the geometries of the icosahedral and cuboctahedral clusters, respectively. For each cluster, the atoms equivalent under the action of the symmetry group form an orbit and we have labeled all the atoms in a given orbit by the number of the orbit. In each case the Mn atom forms orbit no. 1.

For the icosahedral case, we have studied clusters having a central Mn atom surrounded by 12, 24, 32, 42, 44, and 54 Al atoms. Of these, the sizes 12, 24, 42, and 54 correspond to the regular icosahedral (RI) growth. The size 12 corresponds to a first shell (orbit no. 2) of regular icosahedron with radius R_2. Additional 12 or 30 Al atoms lead to the partial filling of the second icosahedral shell of radius R_3 which has 12 summit atoms (orbit no. 3) or 30 edge atoms on regular icosahedron of radius R_4 (orbit no. 4). Adding both 12 summit atoms and 30 edge atoms completes the second shell and the cluster has 54 Al atoms. The size 12, 24, 42, and 54 Al atoms thus include orbits (1+2), (1+2+3), (1+2+4), and (1+2+3+4), respectively.

In addition to the regular icosahedral growth one can add to the first shell of regular icosahedron, 20 Al atoms along the lines joining the central Mn with the centers of the 20 triangular faces of the first shell icosahedron. The resulting structure is a second dodecahedral shell of radius R_5 (orbit no. 5) of 20 atoms and a total size of 32 Al atoms. A third icosahedral shell is then obtained by finally adding 12 Al atoms along lines joining the central Mn atoms with the 12 atoms of the first shell (orbit no. 3). The corresponding size is then 42 Al atoms. We will call

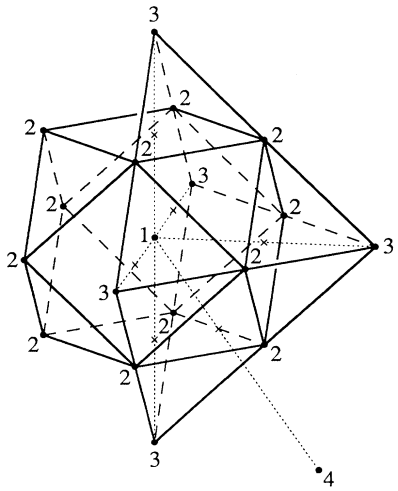

FIG. 2. Geometrical structure of the Al shells (orbits) in the cuboctahedral symmetry of $MnAl_n$. O_1 is the central Mn site labeled by 1. O_2 forms a cuboctahedron of 12 Al sites labeled by 2. O_3 is an octahedron of 6 Al sites labeled by 3 (only 5 sites have been shown in this figure). O_4 is a cube of 8 Al sites labeled by 4 (only 1 site has been shown).

this series the icosahedron-dodecahedron (ID) series. Sizes of 32 and 44 Al atoms include orbits (1+2+5) and (1+2+3+5), respectively.

Finally for the cuboctahedron case we have studied clusters having a central Mn atom surrounded by 12, 18, and 26 Al atoms forming fcc fragments. Size 12 corresponds to the first shell of regular cuboctahedron of radius R_2 (orbit no. 2). Additional 6 Al atoms along the lines joining the central Mn atom with the centers of the 6 square faces of the first cuboctahedron shell give a second octahedral shell of radius R_3 (orbit no. 3) and a total size of 18 Al atoms. Adding 8 Al atoms along the lines joining the central Mn atom with the centers of the 8 triangular faces of the first shell cuboctahedron generates a third cubic shell of radius R_4 (orbit no. 4) and a cluster having 26 Al atoms. We will call this series a cuboctahedron (CO) series. Size 12, 18, and 26 Al atoms include orbits (1+2), (1+2+3), and (1+2+3+4), respectively.

In Table I we give the radii R_n, $n=2,\ldots,5$ for the $MnAl_n$ clusters we have studied.

Both values of R_2 in icosahedral and cuboctahedral symmetries correspond to the equilibrium geometry of $MnAl_{12}$. For bigger clusters, the values of R_2 are kept fixed. Furthermore, the values of R_3, R_4, and R_5 do not correspond to equilibrium geometries but were chosen in such a way that the distance between neighbor Al atoms is in the range of the distance of first- and second-neighbor atoms in bulk Al, i.e., 5.42 and 7.66 a.u., respectively.

III. METHOD OF CALCULATION

The theoretical studies were carried out within the local-spin-density (LSD) approximation of the density-functional formalism. Basically we solve the one-electron Kohn-Sham equations self-consistently. The core effects for the Al atoms were incorporated through the use of the nonlocal pseudopotentials of Bachelet, Hammann, and Schlüter.[11]

For the central Mn, the calculations were carried out in the all-electron scheme since the existing pseudopotentials did not properly reproduce the effect of the core.

For the exchange-correlation potential, we have used the form proposed by Ceperley and Alder[12] which has been parametrized by Perdew and Zunger.[13]

The Kohn-Sham equations for the molecule are[14] (in atomic units)

$$(-\tfrac{1}{2}\nabla^2+V_{\rm ion}+V_H[\rho]+V_{\rm XC}^{\sigma}[\rho_\uparrow,\rho_\downarrow])\psi_{\sigma\nu}=\epsilon_{\sigma\nu}\psi_{\sigma\nu}\ , \quad (1)$$

where $\nu=1,2,\ldots$ is the orbital index, σ represents spin up or down, and the electronic spin density is given by

$$\rho_\sigma(\mathbf{r})=\sum_\nu f_{\sigma\nu}|\psi_{\sigma\nu}(\mathbf{r})|^2$$

and (2)

$$\rho(\mathbf{r})=\sum_\sigma \rho_\sigma(\mathbf{r})\ ,$$

where $0\le f_{\sigma\nu}\le 1$ are the occupation numbers, which are allowed to be nonintegers only for the highest occupied level if it is degenerate. The operators in Eq. (1) correspond to the kinetic energy, ionic pseudopotential, Hartree, and exchange-correlation energies, respectively.

Our studies have been carried out within the framework of the linear combination of atomic orbitals (LCAO) molecular orbital approach. It is useful to briefly point out the structure of the basis functions used by us. These are of the general form

$$G_{l,k}^m(\alpha,\mathbf{r})=Z_l^m(\mathbf{r}-\mathbf{R}_k)\,e^{-\alpha(\mathbf{r}-\mathbf{R}_k)^2}\ , \quad (3)$$

where $\mathbf{R}_k$ is a vector characterizing the position of the atom at the site k, Z_l^m denotes the usual so-called solid harmonic of angular momentum l, m, and α is the exponent of the Gaussian for extension $1/\sqrt{\alpha}$. The basis sets employed in our calculations involved 12s, 7p, and 4d Gaussian functions for Mn atom and 5s and 3p Gaussian functions for the Al atoms. In Table II, we give their exponents α in atomic units. These were obtained via a nonlinear fit of accurate numerical all-electron wave functions for the Mn atom and pseudowave functions (calculated for the same tabulated pseudopotential) for Al atoms. To maintain a high degree of variational freedom, we did not contract the Gaussian basis set.

The quality of our basis is illustrated by the fact that we reproduce the eigenvalues of the accurate numerical wave functions to within an accuracy of 0.13 eV for 3d, 4s, and 4p levels in the case of Mn atom and within an accuracy of 0.01 eV for 3s and 3p levels in Al atom. We would like to point out that our basis set for Mn is different from the earlier basis sets proposed by Roos, Veillard, and Vinot[15] and by Wachters.[16] In particular, our largest s exponent is 914.6 compared to 60 370.5 of Roos, Veillard, and Vinot. This difference is due to the fact that while Roos, Veillard, and Vinot obtain their sets using total energy, our sets are based on actual fits to the numerical atomic functions.

TABLE I. Radii of Al shells (orbits O_2, O_3, O_4, and O_5) for $MnAl_n$ clusters. Radii are given in atomic units.

Cluster	R_2	R_3	R_4	R_5
		RI series		
$MnAl_{12}$	5.0			
$MnAl_{24}$	5.0	10.0		
$MnAl_{42}(a)$	5.0		8.5	
$MnAl_{42}(b)$	5.0		10.0	
$MnAl_{54}$	5.0	10.0	8.5	
		ID series		
$MnAl_{32}(a)$	5.0			8.3
$MnAl_{32}(b)$	5.0			10.0
$MnAl_{44}(a)$	5.0	15.0		8.3
$MnAl_{44}(b)$	5.0	15.0		10.0
$MnAl_{44}(c)$	5.0	10.0		10.0
		CO series		
$MnAl_{12}$	5.4			
$MnAl_{18}$	5.4	7.6		
$MnAl_{26}$	5.4	7.6	13.2	

TABLE II. Gaussian exponents α for Mn and Al atomic orbitals in a.u.

Mn			Al	
s	p	d	s	p
0.9146×10^{3}	0.8736×10^{2}	0.9227×10^{1}	0.2041×10^{1}	0.2500
0.1876×10^{3}	0.2181×10^{2}	0.2459×10^{1}	0.8537	0.1000
0.1225×10^{3}	0.6734×10^{1}	0.6556	0.3571	0.4000×10^{-1}
0.5344×10^{2}	0.1924×10^{1}	0.1747	0.1494	
0.2211×10^{2}	0.6310		0.6250×10^{-1}	
0.1244×10^{2}	0.1012			
0.6280×10^{1}	0.2787×10^{-1}			
0.1176×10^{1}				
0.4053				
0.2311				
0.8346×10^{-1}				
0.3584×10^{-1}				

In order to take advantage of the high symmetry of the system under study (the icosahedral point group I_h and cubic point group O_h), we built up a symmetry-adapted basis set[17] starting from the unsymmetrized basis by using the projection technique of group theory,[18] which decomposes the functional space in orthogonal subspaces.

Let us briefly recall some group theoretical results concerning our method of calculation and analysis. Note that the elements of symmetry group G for the system under consideration are rotations and pseudorotations. Elements $g\in G$ act naturally on space vector. If vector $\mathbf{r}$ corresponds to a point P, g transforms it linearly in a space vector denoted $g\mathbf{r}$ corresponding to the image of P via the rotation or pseudorotation g. Namely, since G is a symmetry group, every rotation or pseudorotation g maps position $\mathbf{R}_i$ of atom no. i onto position $\mathbf{R}_k=g\mathbf{R}_i$ of a certain atom labeled k of the same type as atom i. Then, for each g and for each atom no. i there is a mapping σ_g of i onto k such that

$$g\mathbf{R}_i=\mathbf{R}_{\sigma_g(i)}\ ,\quad \forall g\in G\ ,\quad \text{and}\quad \forall i\ . \tag{4}$$

An orbit is a subset of atoms mapped onto each other by the action of the symmetry group. In other words an orbit is formed by those atoms which are physically equivalent. Clearly, the previous shells of Al atoms form orbits. In the icosahedral case we denote these by O_1 (first shell of a Mn atom), O_2 (second shell of 12 Al atoms), O_3 (third shell of 12 Al atoms), O_4 (fourth shell of 30 Al atoms), and O_5 (fifth shell of 20 Al atoms).

Let us now define the natural action of the symmetry group G onto the functional space $\mathcal{H}$ of the Kohn-Sham spin-up or spin-down orbitals supplied with the usual scalar product.[19] This is given by the unitary operator

$$[U(g)\psi](\mathbf{r})=\psi(g^{-1}\mathbf{r})\ ,\quad \forall g\ ,\quad \text{and}\quad \psi\in\mathcal{H}\ . \tag{5}$$

In particular, the operator $U(g)$ acts on Gaussian basis function $G^m_{l,i}(\alpha,\mathbf{r})$ in the following way, say

$$[U(g)G^m_{l,i}](\alpha,\mathbf{r})=\sum_{m'=-l}^{l} D(g)^l_{m'm}G^{m'}_{l,\sigma_g(i)}(\alpha,\mathbf{r}) \tag{6}$$

because of definition (3) and because of (4). Here, $D(g)^l_{m',m}$ denotes the matrix elements of the irreducible representation of the $O(3)$ group associated to solid harmonic of angular momentum l.

It is clear that linear combinations of basis functions centered on atoms in the same orbit O, with the same angular momentum l and the same exponent α generate linearly a subspace $\mathcal{H}_{O,l,\alpha}$ of $\mathcal{H}$, invariant under the action of G:

$$U(g)\mathcal{H}_{O,l,\alpha}\subseteq\mathcal{H}_{O,l,\alpha},\quad \forall g\ . \tag{7}$$

As a consequence, such invariant subspace $\mathcal{H}_{O,l,\alpha}$ can be decomposed into invariant irreducible subspaces carrying irreducible representations of the symmetry group. For finite group there exists a finite number of sets of equivalent irreducible representations and this number coincides with the number of classes in the group.[20]

In present case, point group I_h containing 120 elements is formed by 10 classes and gives rise to 10 inequivalent irreducible representations. Similarly point group O_h containing 48 elements is formed by 10 classes and also gives rise to 10 inequivalent irreducible representations. Table III gives lists of irreducible representations and corresponding dimensions for both I_h and O_h groups.

Returning to the general situation suppose that $\lambda=1,\ldots,\Lambda$ indexes the sets of equivalent irreducible representations of G. Let us denote by d_λ and χ_λ the dimension and the character of these irreducible representations. Such an index λ is generally called the "type" of the irreducible representations in the corresponding set. Actually Table III labels $A_g, T_{1g}, \ldots$ take place for λ in the case of the I_h group. Similarly labels $A_{1g}, A_{2g}, \ldots$ take place for λ in the case of the O_h group.

Then, for each invariant subspace $\mathcal{H}_{O,l,\alpha}$ and for each type λ of irreducible representation of G there is a uniquely defined null or positive integer a_λ corresponding to the multiplicity of the irreducible representation of type λ occurring in the decomposition of $\mathcal{H}_{O,l,\alpha}$. It is important to point out that for a given $\mathcal{H}_{O,l,\alpha}$ the corresponding sequence of a_λ, $\lambda=1,\ldots,\Lambda$ only depends on

TABLE III. Types and dimensions of the irreducible representations of the I_h and O_h groups.

Group I_h		Group O_h	
Type	Dimen.	Type	Dimen.
A_g	1	A_{1g}	1
T_{1g}	3	A_{2g}	1
T_{2g}	3	E_g	2
G_g	4	T_{1g}	3
H_g	5	T_{2g}	3
A_u	1	A_{1u}	1
T_{1u}	3	A_{2u}	1
T_{2u}	3	E_u	2
G_u	4	T_{1u}	3
H_u	5	T_{2u}	3

the geometry (on the molecular structure) and on the set of basis functions under consideration. More precisely a_λ only depends on the type λ, on the orbit O, and on l.

In Table IV, we give the multiplicity of each irreducible representation of the symmetry group I_h in the invariant subspaces $\mathcal{H}_{O,l,\alpha}$ built up from the basis set Table II and from the orbits $O_1, \ldots, O_5$ previously described in Fig. 1. In Table V, we give the multiplicity of each irreducible representation of the symmetry group O_h in the invariant subspaces $\mathcal{H}_{O,l,\alpha}$ built up from the basis set Table II and from the orbits $O_1, \ldots, O_4$ previously described in Fig. 2.

On the other hand, the whole space $\mathcal{H}$ spanned by the set of basis functions can itself be decomposed into linearly independent irreducible subspaces. An important point is that the subspace $\mathcal{H}^\lambda$ generated by all such irreducible subspaces carrying a representation of type λ are uniquely defined. Actually one can prove that the projector P_λ of $\mathcal{H}$ onto $\mathcal{H}^\lambda$ is expressed as

TABLE IV. Decomposition of invariant subspaces $\mathcal{H}_{O,l,\alpha}$ into irreducible representations of the I_h group. Integer numbers in column A_g give the multiplicity of irreducible representations of type A_g in subspace $\mathcal{H}_{O,l,\alpha}$ and so on.

	Group I_h									
$\mathcal{H}_{O,l,\alpha}$	A_g	T_{1g}	T_{2g}	G_g	H_g	A_u	T_{1u}	T_{2u}	G_u	H_u
Orbit 1										
$l=0$	1	0	0	0	0	0	0	0	0	0
$l=1$	0	0	0	0	0	0	1	0	0	0
$l=2$	0	0	0	0	1	0	0	0	0	0
Orbits 2 and 3										
$l=0$	1	0	0	0	1	0	1	1	0	0
$l=1$	1	1	0	1	2	0	2	1	1	1
Orbit 4										
$l=0$	1	0	0	1	2	0	1	1	1	1
$l=1$	1	2	2	3	4	0	3	3	3	3
Orbit 5										
$l=0$	1	0	0	1	1	0	1	1	1	0
$l=1$	1	1	1	2	3	0	2	2	2	2

TABLE V. Decomposition of invariant subspaces $\mathcal{H}_{O,l,\alpha}$ into irreducible representations of the O_h group. Integer numbers in column A_g give the multiplicity of irreducible representations of type A_{1g} in subspace $\mathcal{H}_{O,l,\alpha}$ and so on.

	Group O_h									
$\mathcal{H}_{O,l,\alpha}$	A_{1g}	A_{2g}	E_g	T_{1g}	T_{2g}	A_{1u}	A_{2u}	E_u	T_{1u}	T_{2u}
Orbit 1										
$l=0$	1	0	0	0	0	0	0	0	0	0
$l=1$	0	0	0	0	0	0	0	0	1	0
$l=2$	0	0	1	0	1	0	0	0	0	0
Orbit 2										
$l=0$	1	0	1	0	1	0	0	0	1	1
$l=1$	1	1	2	2	2	0	1	1	3	2
Orbit 3										
$l=0$	1	0	1	0	0	0	0	0	1	0
$l=1$	1	0	1	1	1	0	0	0	2	1
Orbit 4										
$l=0$	1	0	0	0	1	0	1	0	1	0
$l=1$	1	0	1	1	2	0	1	1	2	1

$$P_\lambda = \frac{d_\lambda}{n_G} \sum_{g \in G} \chi_\lambda(g)^* U(g) , \tag{8}$$

where $U(g)$ denotes the representation defined by (5) and where χ_λ is the character of type λ.[18] The symbol n_G is the number of elements in G. Such a subspace $\mathcal{H}^\lambda$ is called the isotypic component of $\mathcal{H}$ of type λ. Moreover, isotypic components of different types are orthogonal to each other and the set $\mathcal{H}^\lambda$, $\lambda = 1, \ldots, \Lambda$, clearly generates the whole space $\mathcal{H}$.

If one assumes that the spin-up and spin-down electronic densities are separately invariant under the action of the symmetry group, the action U of G commutes with the spin-up and spin-down autocoherent Kohn-Sham operators:

$$[U(g), H^\sigma[\rho_\cdot]] = 0, \quad \forall g . \tag{9}$$

There are several consequences of such commutation rules. First, projectors P_λ and Kohn-Sham operators $H^\sigma[\rho_\cdot]$ commute. Consequently, isotypic components $\mathcal{H}^\lambda$ are stable with respect to the action of the Kohn-Sham operators:

$$H^\sigma[\rho_\cdot]\mathcal{H}^\lambda \subseteq \mathcal{H}^\lambda . \tag{10}$$

Second, each eigenspace of our system carries a representation, irreducible or not, depending on whether the degeneracy is natural or accidental. In fact, a distinction can be made between these two kinds of degeneracies. In reality, each orbital is naturally included in a given isotypic component and a type λ is associated to each orbital. Orbitals associated to the same nonaccidentally degenerate eigenvalue have the same type λ. Finally, the matrix element of $H^\sigma[\rho_\cdot]$ between functions $\phi(\mathbf{r})$ and $\psi(\mathbf{r})$ in different isotypic components cancel.

We are now in position to point out important facts from the contents of Tables IV and V in taking into ac-

count the above mathematical results. Considering icosahedral symmetry, we observe in Table IV that invariant subspace $H_{O,l,\alpha}$ for $O=O_1$ and $l=2$ carry a representation of type H_g. In other words the d states of the Mn atom transform according to type H_g and such states are only coupled with the Al orbitals associated to the same type. Table IV shows that such Al orbitals exist since irreducible representations of type H_g occur in all invariant subspaces $H_{O,l,\alpha}$ for $O=O_n$, $n=2,\ldots,5$ and $l=0,1$. Similarly, the s states of the Mn atoms have type A_g and are only coupled with the Al orbitals having the same type and Table IV shows that such Al orbitals exist since irreducible representations of the type A_g occur in all invariant subspaces $H_{O,l,\alpha}$ for $O=O_n$, $n=2,\ldots,5$ and $l=0,1$. The p states of the Mn atom having type T_{1u} lead to the same conclusion. Finally, we conclude that all Al orbitals having types different from A_g, T_{1u}, and H_g do not couple with the Mn s, p, and d states and will be discarded from the discussion. Note that orbitals of type A_u cannot occur.

For cuboctahedral symmetry the same kind of analysis can be performed. From Table V we observe that invariant subspace $H_{O,l,\alpha}$ for $O=O_1$ and $l=2$ carry representations of types E_g and T_{2g}. In other words the d states of the Mn atom are only coupled with Al orbitals having these previous types. Table V shows that such Al orbitals exist since representations of type E_g occur in all invariant subspaces $H_{O,l,\alpha}$ for $O=O_n$, $n=2,\ldots,4$, and $l=0,1$ and representations of type T_{2g} occur in all invariant subspaces $H_{O,l,\alpha}$ for $O=O_n$, $n=2,\ldots,4$, and $l=0,1$ except for $O=O_3$ and $l=0$. Next, the s states of the Mn atom having A_{1g} type are only coupled with Al orbitals of the same type. Table IV shows that such Al orbitals do exist since representations of type A_{1g} occur in all invariant subspaces $H_{O,l,\alpha}$ for $O=O_n$, $n=2,\ldots,4$, and $l=0,1$ except for $O=O_4$ and for $l=0$. The p states of the Mn atom are of T_{1u} type and lead to the same conclusion. Finally, we conclude that all Al orbitals having types different from A_{1g}, E_g, T_{2g}, and T_{1u} do not couple with Mn s, p, d states and will be removed from the discussion. Note that orbitals of type A_{1u} cannot occur.

The symmetrized basis is built up in the following way. In each invariant subspace $\mathcal{H}_{O,l,\alpha}$ there exist $a_\lambda(O,l)$ irreducible subspaces carrying representations of type λ. Obviously these irreducible subspaces generate the intersection of $\mathcal{H}_{O,l,\alpha}$ with each isotypic component $\mathcal{H}^\lambda$ of $\mathcal{H}$. The symmetrized basis is obtained by choosing a new basis set for functional space $\mathcal{H}$ among functions belonging in the intersections of subspaces $\mathcal{H}_{O,l,\alpha}$ and $\mathcal{H}^\lambda$. Clearly, such symmetrized basis functions have to be labeled by the corresponding type λ and by the corresponding orbit O, angular momentum l, and exponent α.

Since the intersection of subspaces $\mathcal{H}_{O,l,\alpha}$ and $\mathcal{H}^\lambda$ has the dimension $d_\lambda a_\lambda(O,l)$, i.e., the dimension of the irreducible subspace carrying representation of type λ multiplied by the multiplicity of such irreducible subspace in $\mathcal{H}_{O,l,\alpha}$, one still needs an extra index $i=1,\ldots,a(O,l)$ and $k=1,\ldots,d_\lambda$ for a complete unambiguous indexation of such basis functions. Let us denote by $S^\lambda_{i,k,O,l}(\alpha,\mathbf{r})$ such symmetrized basis functions.

It is obvious that a function $S^\lambda_{i,k,O,l}(\alpha,\mathbf{r})$ is a linear combination of the initial Gaussian functions $G^m_{l,k}(\alpha,\mathbf{r})$ centered on the atoms forming the orbit O for fixed exponent α and fixed l. Moreover, such functions transform according to an irreducible representation of type λ with respect to the action of the symmetry group. Consequently, matrix elements of the Kohn-Sham operators between two symmetrized basis functions of different types λ cancel.

There are several advantages of using a symmetrized basis. As previously observed the corresponding matrices for the Kohn-Sham operators $H^\sigma[\rho_\cdot]$ are in block diagonal form. Also symmetry implies definite relations between matrix elements in the same diagonal block. Thus, the number of matrix elements to be calculated and stored is drastically reduced, compared to the unsymmetrized basis, making the problem computationally manageable.

Note that a one-electron orbital which is a linear combination of the symmetrized basis functions $S^\lambda_{i,k,O,l}(\alpha,\mathbf{r})$ for fixed O, l, and λ describes a one-electron l state located on atoms in the orbit O and transforms according to an irreducible representation of type λ. In particular, when λ corresponds to the trivial representation, such an orbital is invariant with respect to the action of the symmetry group: the orbital has the symmetry of the system.

Finally, such a symmetrized basis gives rise to its own scheme of Mulliken population analysis[21] with respect to the orbits O, orbital momenta l, and symmetry types λ. In particular, "gross" population relative to orbit O provides the localization of electrons on the set of atoms forming this orbit. The "gross" population analysis relative to l provides the usual s, p, and d hybridizations. Note that the conventional Mulliken population analysis can sometimes lead to ambiguous results which have to be carefully interpreted. This is particularly true for the analysis based on orbits. In spite of these limitations we have carried out such Mulliken population analysis. For $MnAl_n$ clusters, "gross" population according to orbit O_1 for $l=2$ in principle gives separately the up and down electronic population of the d electron on the Mn site in the cluster. These populations can be related to the magnetic moment on the Mn atom under consideration. In reality, the experiments probe the spin polarization around the Mn site. We, therefore, also provide an alternative estimate of a magnetic moment based on direct numerical integration of the local spin-up and spin-down electronic densities in the vicinity of a Mn atom in spherical regions of various radii.

The Kohn-Sham equations were solved self-consistently by expanding the molecular orbitals in symmetrized basis. The charge density, and the exchange-correlation potential, and energy were fitted by auxiliary Gaussians centered at the atomic and additional sites in between atoms.[22] For details the reader is referred to earlier papers.[23]

IV. ICOSAHEDRAL $MnAl_n$ CLUSTERS

We start this section by a detailed discussion of the electronic structure of $MnAl_{12}$ icosahedral clusters. Let

us recall that the Mn site forms orbit O_1 and that the 12 Al atoms form orbit O_2. The radius R_2 of orbit O_2 has been chosen to correspond to the minimum energy in the icosahedral geometry. In Table VI, we report the energy of the bound state of $MnAl_{12}$ as a function of R_2. The equilibrium was found for $R_2=5.0$ a.u. and the bound state was found to have spin of $\frac{7}{2}$ in the given geometry.

It is important to note that the magnetic moment on the Mn site sensitively depends on the radius R_2 as shown in Table VI. The moment increases as the radius is increased. It is interesting to note that a similar dependence of moment on the interparticle distance was also observed by Dunlap[24] for Fe_{13} clusters.

To further analyze the electronic structure of the $MnAl_{12}$ cluster we have also calculated the electronic structure of the Al_{12} cluster obtained by removing the Mn atom from the $MnAl_{12}$ cluster and keeping R_2 fixed. Such Al_{12} structure has the same symmetry properties as the initial system. The bound state of this Al_{12} cluster was found to have spin 1.

The main results concerning the electronic structure of $MnAl_{12}$ and Al_{12} clusters are summarized in Tables VII and VIII, respectively. Table VII concerning $MnAl_{12}$ gives for each valence one-electron energy level $\epsilon_{\sigma\nu}$ the type of the irreducible representation of I_h associated with the corresponding eigenspace, the s, p, and d hybridization and the "gross" Mulliken population on orbits O_1 and O_2. The core one-electron energy levels of the Mn atom have been removed from the table. Table VIII summarizes the corresponding information on the Al_{12} cluster.

In $MnAl_{12}$, starting from the lowest one-electron energy level, all the orbitals are occupied by one electron. The occupation coincides with the dimension of the irreducible representation corresponding to the energy level. The highest occupied energy level is partially occupied (down-spin level no. 7 carrying representation H_g of dimension 5) by one electron. To obtain a total electronic density compatible with the symmetry we have given an occupation of 0.2 to each of the five orbitals of this level. Because of the need of partial occupation of this energy level, we can expect that real equilibrium geometry of the cluster will undergo a small Jahn-Teller distortion breaking the icosahedral symmetry. These effects are not relevant for the present discussion.

TABLE VI. Variation of the magnetic moment μ of the Mn atom (from Mulliken population analysis) and of the energy E for icosahedral $MnAl_{12}$ as a function of the radius R_2 of the O_2 orbit. The energy is given relative to the equilibrium energy.

	$MnAl_{12}$ (I_h)								
R_2 (a.u.)	4.8	4.9	5.0	5.1	5.2	5.3	5.4	5.5	5.6
μ (μ_B)	3.11	3.21	3.32	3.37	3.50	3.59	3.66	3.75	3.83
E (eV)	0.64	0.15	0.00	0.14	0.51	1.06	1.76	2.56	3.44

To analyze the electronic coupling between the Mn atom and the Al atoms in $MnAl_{12}$, we have reproduced separately in Figs. 3 and 4 the spin-up and spin-down one-electron energy levels with the corresponding type of irreducible representation of I_h for Al, Al_{12}, $MnAl_{12}$, and Mn.

The orbitals of $MnAl_{12}$ come from coupling between the orbitals of the Mn atom and Al_{12} cluster. Note that

TABLE VII. One-electron energy levels for icosahedral $MnAl_{12}$. For each occupied level we give the energy (Ha), the type, the degeneracy, the occupation per orbital, the s, p, and d hybridizations, the Mulliken population per orbital on orbits O_1 and O_2, and finally Δ_{Mn}, the local electronic contribution per orbital in a spherical region of radius $r=3.0$ a.u. around the Mn atom. The core one-electron energy levels of the Mn atom have been removed.

				Icosahedral $MnAl_{12}$ (I_h)						
Level	Energy	Type	Degen.	Occ.	s	p	d	O_1	O_2	Δ_{Mn}
				Spin-up orbitals						
1	−0.510	A_g	1	1.0	0.93	0.07	0.00	0.62	0.38	0.231
2	−0.429	T_{1u}	3	1.0	1.19	−0.19	0.00	−0.64	1.64	0.119
3	−0.352	H_g	5	1.0	0.56	0.10	0.34	0.35	0.65	0.330
4	−0.256	A_g	1	1.0	1.09	−0.09	0.00	−0.21	1.21	0.212
5	−0.246	H_g	5	1.0	0.32	0.09	0.59	0.59	0.41	0.592
6	−0.215	T_{2u}	3	1.0	1.17	−0.17	0.00	0.00	1.00	0.006
7	−0.204	G_u	4	1.0	0.00	1.00	0.00	0.00	1.00	0.009
8	−0.186	T_{1u}	3	1.0	0.08	0.92	0.00	0.54	0.46	0.157
				Spin-down orbitals						
1	−0.496	A_g	1	1.0	0.88	0.12	0.00	0.27	0.73	0.231
2	−0.419	T_{1u}	3	1.0	1.36	−0.36	0.00	−0.92	1.92	0.119
3	−0.330	H_g	5	1.0	0.75	0.11	0.14	0.14	0.86	0.151
4	−0.236	A_g	1	1.0	1.09	−0.09	0.00	−0.13	1.13	0.206
5	−0.203	T_{2u}	3	1.0	1.20	−0.20	0.00	0.00	1.00	0.007
6	−0.198	G_u	4	1.0	0.00	1.00	0.00	0.00	1.00	0.009
7	−0.180	H_g	5	0.2	0.15	0.19	0.66	0.65	0.35	0.634

TABLE VIII. One-electron energy levels for icosahedral Al_{12}. For each occupied level we give the energy (*Ha*), the type, the degeneracy, the occupation per orbital, the *s* and *p* hybridizations, and finally Δ_{Mn}, the local electronic contribution per orbital in a spherical region of radius $r=3.0$ a.u. around the position of the removed Mn atom.

Level	Energy	Type	Degen.	Occ.	*s*	*p*	Δ_{Mn}
			Icosahedral Al_{12} (I_h)				
			Spin-up orbitals				
1	−0.478	A_g	1	1.0	0.82	0.18	0.151
2	−0.412	T_{1u}	3	1.0	0.88	0.12	0.082
3	−0.316	H_g	5	1.0	0.84	0.16	0.033
4	−0.219	A_g	1	1.0	0.22	0.78	0.178
5	−0.212	T_{2u}	3	1.0	1.15	−0.15	0.006
6	−0.202	G_u	4	1.0	0.00	1.00	0.009
7	−0.162	T_{1u}	3	2/3	−0.02	1.02	0.107
8	−0.123	H_g	5	0.0	0.18	0.82	
			Spin-down orbitals				
1	−0.473	A_g	1	1.0	0.83	0.17	0.146
2	−0.408	T_{1u}	3	1.0	0.87	0.13	0.081
3	−0.312	H_g	5	1.0	0.83	0.17	0.033
4	−0.210	A_g	1	1.0	0.22	0.78	0.175
5	−0.206	T_{2u}	3	1.0	1.18	−0.18	0.006
6	−0.199	G_u	4	1.0	0.00	1.00	0.009
7	−0.153	T_{1u}	3	0.0	−0.02	1.02	
8	−0.116	H_g	5	0.0	0.20	0.80	

the orbitals of the Mn atom and the orbitals of the Al_{12} cluster are both represented in the functional space for the $MnAl_{12}$ cluster. The Mn orbitals will have zero components on the basis functions centered on Al sites and conversely the Al_{12} orbitals will have zero components on the basis functions centered on the Mn atom. Next, consider the Kohn-Sham operators for $MnAl_{12}$ provided by the spin-up and spin-down electronic densities which are the sums of the corresponding electronic densities from the isolated Mn atom and the isolated Al_{12} cluster. Notice that these initial orbitals and Kohn-Sham operators do not satisfy the self-consistency condition. Relaxation to self-consistency gives an illustration of the coupling mechanism which occurs in two ways. First, a direct one, via a linear combination of orbitals from the Mn atom and the Al_{12} cluster to form new eigenfunctions of the Kohn-Sham operators.

Second, an indirect one, because of the relaxation to the self-consistency modifying Kohn-Sham operators themselves by keeping the symmetry properties unchanged. All the selection rules from the symmetry hold in during such processes.

From Table VIII we observe that levels 5 and 6 for up and down spins in Al_{12} have types T_{2u}, and G_u, respectively. As previously mentioned, these orbitals cannot couple with the Mn orbitals. In $MnAl_{12}$ these orbitals correspond to orbitals from energy levels 6 and 7 up and 5 and 6 down. Note the small difference in the corresponding energy levels between both clusters (less than 0.003 a.u.). Further, these orbitals contribute only $\Delta_{Mn}=0.01$ electron per orbital in the Mn spherical region of radius 3.0 a.u. and can be discarded from the discussion. It is important to point out that the previous observed facts are true for the whole sect of icosahedral $MnAl_n$ clusters studied here. All the orbitals with a type different from A_g, T_{1u}, and H_g have negligible electronic contributions in the Mn region, actually less than 0.01 electron per orbitals. We shall call such orbitals pure Al orbitals.

Consequently, we focus the discussion on the orbitals of types A_g, T_{1u}, and H_g which can, respectively, couple

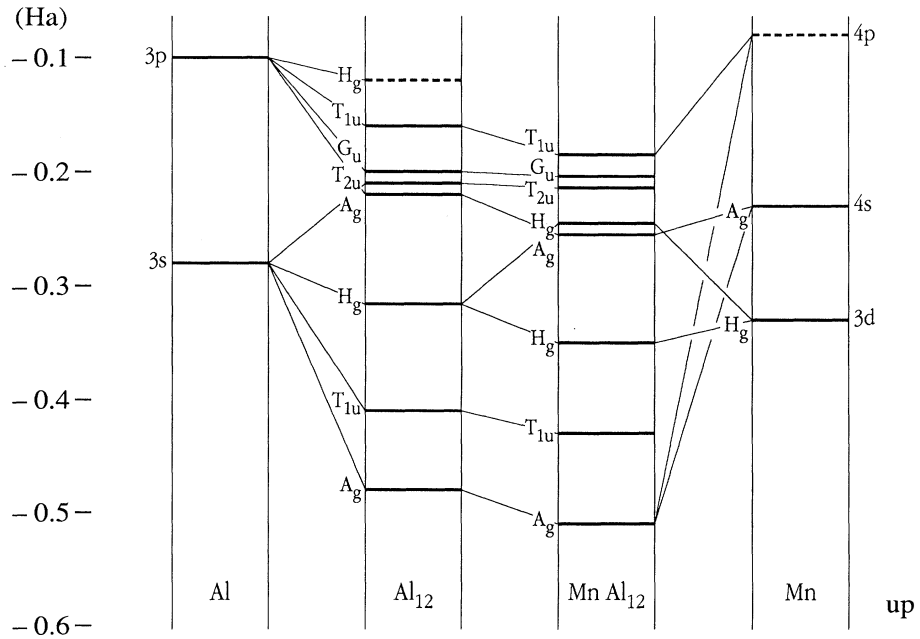

FIG. 3. Spin-up energy levels for Al_{12} and $MnAl_{12}$ clusters and for Mn atom. For reference energy levels of spin-symmetrized Al atom have been shown on the left side of the figure. The occupied energy levels are represented by bold lines and empty levels by bold dashed lines. Lines joining energy levels of Al_{12} and Mn atoms with those of $MnAl_{12}$ correspond to mixing. Lines joining the Al atom with Al_{12} levels underline the *s* and *p* character of levels (*s*, *p* Al preband).

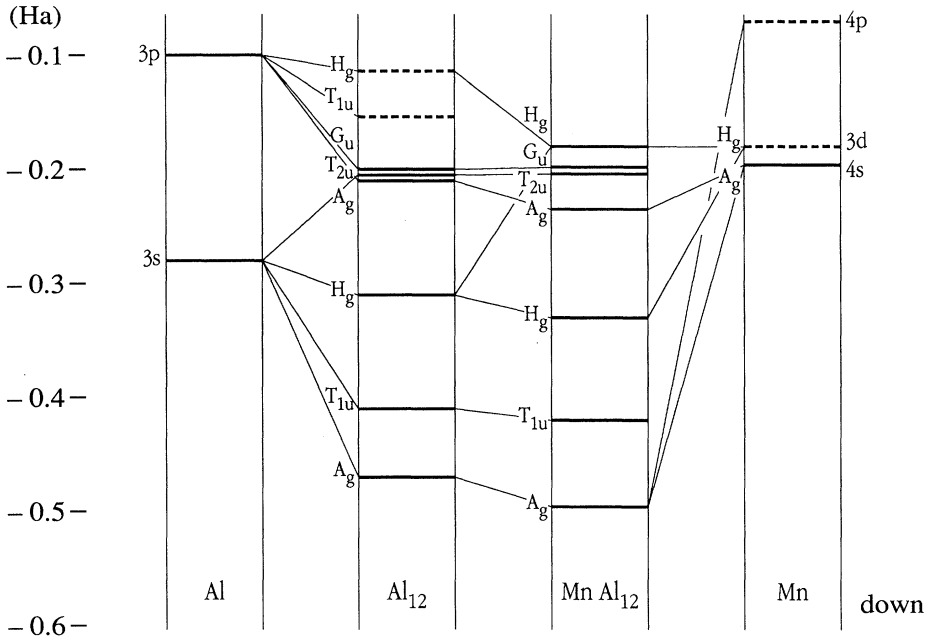

FIG. 4. Spin-down energy levels for Al_{12} and $MnAl_{12}$ clusters, and for the Mn atom. The convention is same as for spin-up one-electron energy levels.

with the *s*, *p*, and *d* states of the Mn atom. In Al_{12}, the orbitals from spin-up and spin-down level nos. 1 and 4 have type A_g and couple with the 4*s* state in Mn. The corresponding orbitals in the $MnAl_{12}$ cluster are the spin-up and spin-down orbitals from level nos. 1 and 4 and exhibit a strong coupling between the 4*s* state of Mn and the A_g states of Al_{12}. All of them contribute for about 0.88 electron in the Mn region but about $+0.06\mu_B$ for the local magnetic moment. Next, the spin-up and spin-down orbitals from the levels nos. 2 and 7 in Al_{12} have type T_{1u} and couple with the *p* states in Mn. Corresponding occupied orbitals in $MnAl_{12}$ are the spin-up orbitals from level nos. 2 and 8 and the spin-down orbitals from level no. 2. All of them contribute around 1.19 elec-

TABLE IX. Total *s*, *p*, and *d* hybridization and local electronic contribution Δ_{Mn} in a spherical region of radius 3 a.u. around the Mn atom for the spin-up and spin-down orbitals of types A_g, T_{1u}, and H_g in $MnAl_n$ icosahedral clusters in RI series. In column μ we have given the corresponding local magnetic moment in μ_B units. The contributions from the core electrons in the Mn atom have been removed.

		Icosahedral symmetry: RI series								
		Spin-up orbitals				Spin-down orbitals				
	Type	*s*	*p*	*d*	Δ_{Mn}	*s*	*p*	*d*	Δ_{Mn}	μ
Mn	A_g	1.00	0.00	0.00	0.35	1.00	0.00	0.00	0.29	0.06
	T_{1u}	0.00	0.00	0.00	0.00	0.00	0.00	0.00	0.00	0.00
	H_g	0.00	0.00	5.00	4.76	0.00	0.00	0.00	0.00	4.76
$MnAl_{12}$	A_g	2.01	−0.01	0.00	0.44	1.97	0.03	0.00	0.44	0.00
	T_{1u}	3.77	2.23	0.00	0.83	4.05	−1.05	0.00	0.36	0.47
	H_g	4.40	0.93	4.67	4.61	3.89	0.75	1.36	1.39	3.22
$MnAl_{24}$	A_g	2.35	0.65	0.00	0.43	2.32	0.68	0.00	0.42	0.01
	T_{1u}	1.40	7.60	0.00	0.58	1.06	7.94	0.00	0.57	0.01
	H_g	8.18	7.96	3.86	3.94	8.10	4.65	2.25	2.39	1.55
$MnAl_{42}(a)$	A_g	2.78	0.22	0.00	0.41	2.78	0.22	0.00	0.41	0.00
	T_{1u}	7.81	4.20	0.00	0.63	7.71	4.29	0.00	0.63	0.00
	H_g	7.48	9.56	2.97	3.21	7.46	9.65	2.89	3.14	0.07
$MnAl_{42}(b)$	A_g	3.34	−0.34	0.00	0.41	3.36	−0.36	0.00	0.41	0.00
	T_{1u}	6.36	2.64	0.00	0.56	6.63	5.37	0.00	0.59	−0.03
	H_g	15.02	6.32	3.66	3.72	13.61	4.82	2.57	2.67	1.05
$MnAl_{54}$	A_g	−2.55	6.56	0.00	0.39	−2.35	6.35	0.00	0.39	0.00
	T_{1u}	1.48	13.52	0.00	0.55	4.19	7.82	0.00	0.52	0.03
	H_g	8.19	18.77	3.04	3.24	8.31	18.70	2.99	3.21	0.03

TABLE X. Total s, p, and d hybridization and local electronic contribution Δ_{Mn} into a spherical region of radius 3 a.u. around the Mn atom for the spin-up and spin-down orbitals of types A_g, T_{1u}, and H_g in $MnAl_n$ icosahedral clusters in ID series. In column μ we have given the corresponding local magnetic moment in μ_B units. The contributions from the core electron in the Mn atom have been removed.

		Icosahedral symmetry: ID series								
		Spin-up orbitals				Spin-down orbitals				
	Type	s	p	d	Δ_{Mn}	s	p	d	Δ_{Mn}	μ
Mn	A_g	1.00	0.00	0.00	0.35	1.00	0.00	0.00	0.29	0.06
	T_{1u}	0.00	0.00	0.00	0.00	0.00	0.00	0.00	0.00	0.00
	H_g	0.00	0.00	5.00	4.76	0.00	0.00	0.00	0.00	4.76
$MnAl_{12}$	A_g	2.01	−0.01	0.00	0.44	1.97	0.03	0.00	0.44	0.00
	T_{1u}	3.77	2.23	0.00	0.83	4.05	−1.05	0.00	0.36	0.47
	H_g	4.40	0.93	4.67	4.61	3.89	0.75	1.36	1.39	3.22
$MnAl_{32}(a)$	A_g	3.32	−0.32	0.00	0.48	3.29	−0.29	0.00	0.45	0.03
	T_{1u}	−16.73	22.73	0.00	0.44	−15.62	24.62	0.00	0.66	−0.22
	H_g	14.70	1.00	4.31	4.48	14.39	0.20	1.41	1.66	2.82
$MnAl_{32}(b)$	A_g	3.19	−0.19	0.00	0.41	3.17	−0.17	0.00	0.41	0.00
	T_{1u}	4.70	4.30	0.00	0.58	4.62	4.38	0.00	0.58	0.00
	H_g	9.48	7.39	3.13	3.16	9.48	7.25	3.27	3.30	−0.14
$MnAl_{44}(a)$	A_g	4.99	−0.99	0.00	0.43	5.00	−1.00	0.00	0.43	0.00
	T_{1u}	−16.66	28.66	0.00	0.56	−16.65	29.65	0.00	0.58	−0.02
	H_g	19.37	2.64	3.00	3.22	19.13	2.96	2.91	3.15	0.07
$MnAl_{44}(b)$	A_g	5.02	−1.02	0.00	0.41	5.02	−1.02	0.00	0.41	0.00
	T_{1u}	7.66	4.34	0.00	0.57	7.62	4.38	0.00	0.57	0.00
	H_g	14.19	7.67	3.14	3.16	14.24	7.48	3.28	3.30	−0.14
$MnAl_{44}(c)$	A_g	3.74	0.26	0.00	0.40	3.72	0.28	0.00	0.40	0.00
	T_{1u}	11.57	0.43	0.00	0.57	11.62	0.38	0.00	0.57	0.00
	H_g	13.40	8.54	3.07	3.18	12.21	6.69	3.11	3.22	−0.04

tron in the Mn region and about $+0.47\mu_B$ to the local magnetic moment. Finally, the spin-up and spin-down orbitals from level nos. 3 and 8 have type H_g and couple with $3d$ states in Mn. The corresponding orbitals in $MnAl_{12}$ are the spin-up orbitals from levels nos. 3 and 5 and the spin-down oribitals from level nos. 3 and 7. Actually, Table VII shows that the spin-up orbitals from level no. 3 have a dominant Al character with a contribution of around 1.65 electron in the Mn region and the spin-up orbitals from level no. 5 have a dominant Mn character with a contribution of about 2.96 electrons in the Mn region. Similarily, the spin-down orbitals from level no. 3 have dominant Al character with a contribution of about 0.75 electron in the Mn region. The partially occupied spin-down energy level no. 7 has clearly dominant Mn character with a contribution of 0.63 electron in the Mn region. The total contribution of the H_g orbitals in the Mn region is around 5.99 electrons and $+3.22\mu_B$.

In Figs. 3 and 4, we present the one-electron energy levels of Al_{12} and $MnAl_{12}$ clusters and of the Mn atom indicating corresponding type. The energy levels of the spin-symmetrized Al atom are also shown for reference. We have drawn lines joining coupled one-electron energy levels from the Al_{12} cluster and the Mn atom to the $MnAl_{12}$ cluster.

A comparison of the one-electron energy levels in the Mn atom and in the Al_{12} cluster with the one-electron energy levels in the $MnAl_{12}$ cluster shows that the coupling between the Mn orbitals and the Al orbitals having types A_g, T_{1u}, and H_g is significant. Further, a comparison of the local spin-up and -down electronic contributions Δ_{Mn} from A_g orbitals (given in Table IX) in a spherical region of radius 3 a.u. centered on the Mn atom in the $MnAl_{12}$ cluster with the corresponding contribution in a single

TABLE XI. Local magnetic moment μ on the Mn atom from Mulliken population analysis, number of H_g electrons, p hybridization of the H_g electrons, corresponding p hybridization per H_g electron, and total magnetic moment for icosahedral $MnAl_n$ clusters in the RI and ID series.

Cluster	μ	Nb. H_g elec.	Total p hyb.	p hyb. elec.	Total μ
		RI series			
$MnAl_{12}$	3.31	16	1.68	0.10	3.5
$MnAl_{24}$	1.61	35	12.61	0.36	2.5
$MnAl_{42}(a)$	0.08	40	19.21	0.48	1.5
$MnAl_{42}(b)$	1.09	46	11.14	0.24	0.5
$MnAl_{54}$	0.05	60	37.47	0.62	1.5
		ID series			
$MnAl_{32}(a)$	2.90	36	1.20	0.03	0.5
$MnAl_{32}(b)$	−0.14	40	14.64	0.37	1.5
$MnAl_{44}(a)$	0.09	50	5.6	0.11	1.5
$MnAl_{44}(b)$	−0.14	50	15.15	0.30	1.5
$MnAl_{44}(c)$	−0.04	47	15.23	0.32	1.5

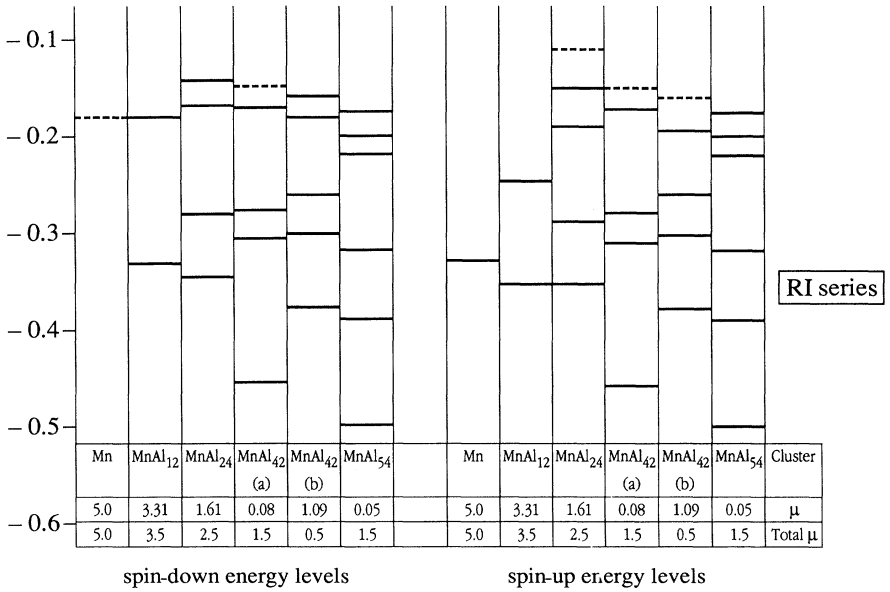

FIG. 5. Comparison of one-electron energy levels of type H_g for the $MnAl_n$ clusters in the RI series. Dashed levels are empty. Line μ refers to the local magnetic moment on the Mn atom from the Mulliken population analysis and line "Total μ" refers to the total magnetic moment (or spin) of the cluster in μ_B units.

Mn atom shows that Mn-Al coupling is responsible for a significant transfer of 4*s* electrons in Mn. We observe a local increase of about 0.24 4*s* electron from 0.64 for the Mn atom to 0.88 electron for the $MnAl_{12}$ cluster. A similar effect occurs for H_g orbitals. We have a local decrease of 0.15 3*d* spin-up electron from 4.76 for the Mn atom to 4.61 electrons for $MnAl_{12}$ and a local increase of 1.39 4*s* spin-down electrons from 0.00 for the Mn atom. Finally we observe that the T_{1u} orbitals contain a significant local contribution of about 1.19 4*p* electrons in the Mn region. In spite of the previous significant coupling between the Al orbitals of types A_g, T_{1u}, and H_g and the *s*, *p*, and *d* states in the Mn atom, respectively, the main contribution to the change of the local magnetic moment in the Mn region comes from the coupling between the Al orbitals of type H_g and the *d* orbitals of the Mn atom. Actually, if we refer to Tables IX and X we observe a similar effect for the whole set of icosahedral $MnAl_n$ clusters. Contributions to the change of the local magnetic moment for the Mn atom never exceed $0.06\mu_B$ for the whole set of A_g orbitals. Further, contributions to the change of local magnetic moment for the Mn atom

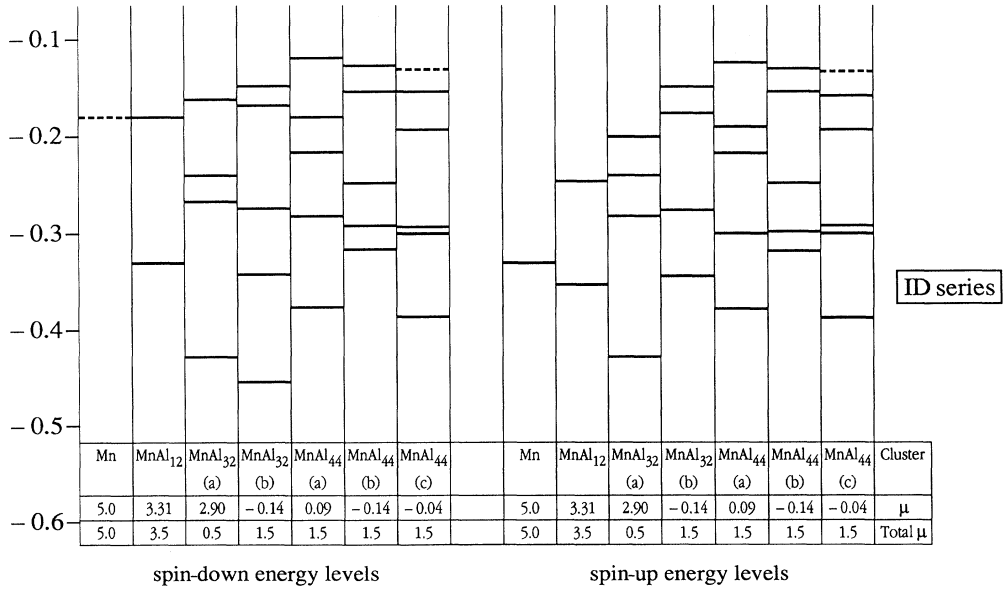

FIG. 6. Comparison of one-electron energy levels of type H_g for the $MnAl_n$ clusters in the ID series. Dashed levels are empty.

never exceed $0.03\mu_B$ for the whole set of T_{1u} orbitals except for $MnAl_{12}$ and $MnAl_{32}(a)$ where the change is about 0.47 and $0.22\mu_B$, respectively.

If we consider the total s, p hybridization of the orbitals of type H_g given in Tables IX and X, we observe an increase of the p characters together with a decrease of the local magnetic moment on the Mn atom as a function of the size. In the RI series, the p hybridization per electron from $MnAl_{12}$ to $MnAl_{54}$ varies from 0.10 to 0.62 for a local magnetic moment varying from 3.31 to $0.05\mu_B$. In the ID series, from $MnAl_{12}$ to $MnAl_{44}$, the p hybridization varies from 0.10 to 0.32 for a local magnetic moment varying from 3.31 to $-0.14\mu_B$. Here, it is important to point out that negative value for the local magnetic moment is not meaningless because all our calculations have been carried out with the convention that the number of spin-up electrons is equal or exceeds the number of spin-down electrons. The results concerning the previous discussion have been summarized in Table XI.

In spite of the strong sensitivity of the local magnetic moment to the geometry, as shown, a comparison between $MnAl_{42}(a)$ and (b), and between $MnAl_{32}(a)$ and (b), shows that an increasing p character of orbitals of type H_g gives rise to a decrease of the local magnetic moment on the Mn atom. In other words, the mechanism of the quenching of the magnetic moment on the Mn atom is mainly related to the occurrence of p orbitals of Al with the symmetry properties of type H_g, the only symmetry allowing mixing with d orbitals of Mn. It is important to compare the behavior of the magnetic moment on the Mn site with the behavior of the one-electron energy spectrum associated with type H_g. To make it more transparent we have shown in Figs. 5 and 6 these spectra together with the corresponding magnetic moment on the Mn atom in the $MnAl_n$ clusters for the RI and ID series.

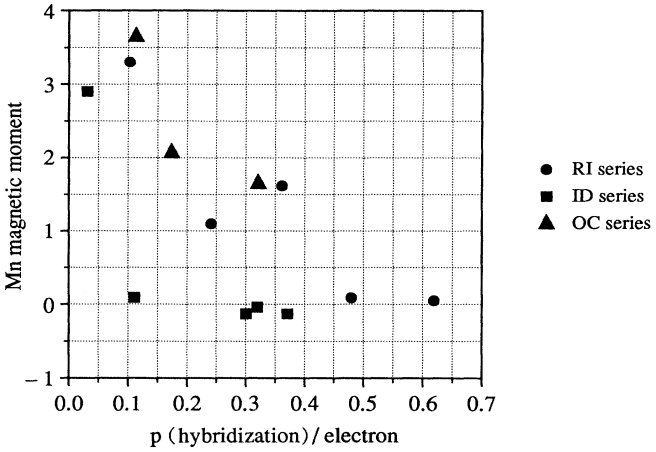

FIG. 7. Plot of the magnetic moment on the Mn site according to the p hybridization per electron from the orbitals of type H_g for the $MnAl_n$ clusters.

TABLE XII. Local magnetic moment in μ_B units into spherical regions centered on the Mn atom in icosahedral $MnAl_n$ for radii 0.5, 1.0, 1.5, 2.0, 2.5, and 3.0 a.u. The contributions from the orbitals of type H_g and the total contributions from the whole set of orbitals are given.

		Icosahedral symmetry: RI and ID series					
	Type	0.5	1.0	1.5	2.0	2.5	3.0
Mn	H_g	0.476	2.363	3.695	4.410	4.764	4.886
	Total	0.480	2.391	3.719	4.451	4.819	4.953
$MnAl_{12}$	H_g	0.304	1.512	2.381	2.874	3.126	3.208
	Total	0.312	1.560	2.431	2.994	3.421	3.748
$MnAl_{24}$	H_g	0.154	0.766	1.199	1.436	1.541	1.550
	Total	0.156	0.777	1.208	1.448	1.561	1.575
$MnAl_{42}(a)$	H_g	0.008	0.037	0.057	0.067	0.070	0.068
	Total	0.008	0.038	0.058	0.068	0.070	6.091
$MnAl_{42}(b)$	H_g	0.104	0.516	0.809	0.971	1.043	1.050
	Total	0.105	0.521	0.813	0.972	1.038	1.031
$MnAl_{54}$	H_g	0.004	0.018	0.028	0.033	0.035	0.032
	Total	0.004	0.020	0.030	0.036	0.043	0.053
$MnAl_{32}(a)$	H_g	0.275	1.365	2.143	2.575	2.778	2.818
	Total	0.274	1.369	2.142	2.551	2.688	2.617
$MnAl_{32}(b)$	H_g	−0.014	−0.068	−0.106	−0.127	−0.136	−0.136
	Total	−0.014	−0.069	−0.108	−0.130	−0.142	−0.147
$MnAl_{44}(a)$	H_g	0.010	0.050	0.076	0.085	0.084	0.075
	Total	0.011	0.051	0.075	0.082	0.073	0.051
$MnAl_{44}(b)$	H_g	−0.013	−0.063	−0.099	−0.120	−0.130	−0.133
	Total	−0.013	−0.064	−0.100	−0.122	−0.135	−0.141
$MnAl_{44}(c)$	H_g	−0.003	−0.017	−0.026	−0.030	−0.032	−0.031
	Total	−0.003	−0.017	−0.026	−0.032	−0.036	−0.039

TABLE XIII. Total s, p, and d hybridization and local electronic contribution Δ_{Mn}, in a spherical region of radius 3 a.u. centered on the Mn atom for the spin-up and spin-down orbitals of types A_{1g}, T_{1u}, E_g, and T_{2g} in $MnAl_n$ cuboctahedral clusters in CO series. In column μ we have given the corresponding local magnetic moment in μ_B units. The contributions from the core orbitals of the Mn atom have been removed.

		Cuboctahedral symmetry: CO series								
		Spin-up orbitals				Spin-down orbitals				
	Type	s	p	d	Δ_{Mn}	s	p	d	Δ_{Mn}	μ
Mn	A_{1g}	1.00	0.00	0.00	0.35	1.00	0.00	0.00	0.29	0.06
	T_{1u}	0.00	0.00	0.00	0.00	0.00	0.00	0.00	0.00	0.00
	E_g	0.00	0.00	2.00	1.90	0.00	0.00	0.00	0.00	1.90
	T_{2g}	0.00	0.00	3.00	2.86	0.00	0.00	0.00	0.00	2.86
$MnAl_{12}$	A_{1g}	1.76	0.24	0.00	0.44	1.73	0.28	0.00	0.40	0.04
	T_{1u}	3.38	5.62	0.00	0.64	3.65	2.35	0.00	0.31	0.33
	E_g	1.63	0.48	1.89	1.86	1.58	0.25	0.17	0.19	1.67
	T_{2g}	2.56	0.64	2.80	2.74	2.43	0.71	0.86	0.85	1.89
$MnAl_{18}$	A_{1g}	3.03	−0.03	0.00	0.42	3.01	−0.01	0.00	0.39	0.03
	T_{1u}	7.29	1.71	0.00	0.40	7.29	1.71	0.00	0.38	0.02
	E_g	3.80	0.55	1.65	1.67	3.74	0.77	0.50	0.56	1.11
	T_{2g}	2.79	0.85	2.36	2.33	2.82	1.75	1.43	1.42	0.91
$MnAl_{26}$	A_{1g}	4.05	−0.05	0.00	0.39	4.07	−0.07	0.00	0.37	0.02
	T_{1u}	10.73	1.27	0.00	0.37	10.63	1.37	0.00	0.36	0.01
	E_g	3.74	2.60	1.66	1.69	3.84	1.50	0.66	0.71	0.98
	T_{2g}	5.83	3.98	2.19	2.17	5.79	3.68	1.52	1.51	0.66

Contrary to the expectation, we observe that the structure and the behavior of the previously mentioned spectra do not take a dominant part in the mechanism of the quenching of the Mn magnetic moment. The main determining factor is the p hybridization of orbital of type H_g. This trend is clear from Fig. 7 where we have plotted the magnetic moment on the Mn atom and the corresponding p hybridization per electron from the occupied H_g orbitals.

To end this section we give in Table XII the detailed distribution of the magnetic moment on the Mn site into spherical regions of radius 0.5–3.0 a.u. Actually, this is the most convenient form for comparing our results with experimental data since the magnetic moment on the Mn site is never directly measured but determined through a model referring to the magnetic moment distribution in the isolated Mn atom.

V. CUBOCTAHEDRAL $MnAl_n$ CLUSTERS

Our results for the cuboctahedral symmetry present the same basic features as for the icosahedral case. We find that the orbitals of type different from types A_{1g}, T_{1g}, E_g, and T_{2g} have no coupling with s, p, and d orbitals of the Mn atom. All of these give a contribution of less than $\Delta_{Mn}=0.01$ electron per orbital. Since these orbitals give rise to a negligible contribution, we focus the discussion on the orbitals of type A_{1g} which have coupling with the 4s orbitals of the Mn atom, on the orbitals of type T_{1g} which have coupling with the 4p orbitals of the Mn atom, and on orbitals of types E_g and T_{2g} which have coupling with the d orbitals of the Mn atom. Our main findings concerning the local electronic contribution from these orbitals at the site of the Mn atom are summarized in Table XIII.

We notice that in the CO series, as we go from $MnAl_{12}$ to $MnAl_{26}$, the local electronic contributions from the A_{1g} orbitals at the Mn site decrease monotonically from 0.84 to 0.76 electron compared with 0.64 electron for the case of a single Mn atom and give rise to a local magnetic moment of less than $0.04\mu_B$. Local electronic contributions from the T_{1u} orbitals decrease monotonically from 0.95 to 0.73 electron giving rise to a local magnetic moment of about $0.33\mu_B$ for $MnAl_{12}$ but less than $0.02\mu_B$ for other sizes. Finally, the local electronic contributions from the orbitals E_g and T_{2g} increase with size. The corresponding values are, respectively, 5.64, 5.98, and 6.08 electrons compared with 5.0 electrons in a single Mn atom. On the other hand, corresponding local magnetic moments are 3.56, 2.02, and $1.64\mu_B$. We conclude that the coupling between the E_g and T_{2g} orbitals of Al and the d orbitals of the Mn atom is largely responsible for the quenching of the magnetic moment on the Mn site.

TABLE XIV. Local magnetic moment μ on the Mn atom from Mulliken population analysis, number of E_g and T_{2g} electrons, p hybridization of the E_g and T_{2g} electrons, corresponding p hybridization per H_g and T_{2g} electron, and total magnetic moment for cuboctahedral $MnAl_n$ clusters in the ID series.

	CO series				
Cluster	μ	Nb. E_g and T_{2g} elec.	Total p hyb	p hyb/elec.	Total μ
$MnAl_{12}$	3.66	16	2.24	0.14	3.5
$MnAl_{18}$	2.08	23	3.92	0.17	0.5
$MnAl_{26}$	1.67	37	11.76	0.32	1.5

TABLE XV. Local magnetic moment in μ_B units in the spherical region around the Mn atom in cuboctahedral $MnAl_n$ for various radii (a.u.). Contributions from orbitals of type E_g and T_{2g} and total contributions are given.

	Cuboctahedral symmetry: CO series						
	Type	0.5	1.0	1.5	2.0	2.5	3.0
Mn	E_g	0.190	0.945	1.478	1.764	1.906	1.954
	T_{2g}	0.286	1.418	2.217	2.646	2.858	2.932
	Total	0.480	2.391	3.719	4.451	4.819	4.953
$MnAl_{12}$	E_g	0.157	0.784	1.234	1.488	1.619	1.670
	T_{2g}	0.181	0.899	1.411	1.695	1.838	1.887
	Total	0.345	1.722	2.682	3.265	3.654	3.992
$MnAl_{18}$	E_g	0.105	0.522	0.821	0.990	1.076	1.106
	T_{2g}	0.093	0.459	0.715	0.851	0.907	0.905
	Total	0.199	0.994	1.547	1.857	2.013	2.053
$MnAl_{26}$	E_g	0.093	0.463	0.729	0.878	0.951	0.974
	T_{2g}	0.066	0.327	0.512	0.610	0.652	0.652
	Total	0.160	0.799	1.248	1.498	1.619	1.646

Further, in Table XIV we finally observe that the quenching itself is strongly related to the occurrence of p orbitals of Al with symmetry types E_g and T_{2g}.

To sum up, we give in Table XV the detailed distribution of the magnetic moment into spherical regions centered on the Mn atom for radii 0.5–3.0 a.u.

VI. CONCLUSIONS

To conclude, we have used clusters to investigate if the local symmetry of Al atoms in a MnAl system could lead to magnetic Mn sites. We have presented results for two geometries, namely, icosahedral and cuboctahedral clusters. The former is motivated by the symmetry exhibited by MnAl quasicrystals while the latter corresponds to the symmetry group possessed by bulk Al. In both cases we find that the symmetry allows a mixing between the Mn d and the Al sp states and that the moment on the Mn atom depends sensitively on this mixing. The extent of the mixing, however, depends on the interatomic distances and on the cluster size. For small clusters, the mixing is small and the Mn sites do carry a finite moment. This was taken, by previous authors[9] who carried out calculations on only small icosahedral clusters to imply that probably the icosahedral symmetry can stabilize the Mn moment. This is the limitation of cluster calculations. One has to be careful about the cluster size before accepting these implications. In fact, in both geometries, the magnetic moment is zero irrespective of the symmetry if one goes to reasonably big clusters. This result is, incidently, consistent with experiments on Mn_xAl_{1-x} alloys with low Mn content (x smaller than 2%) which show that Mn sites do not carry any magnetic moment at these concentrations.[8]

In view of the present results, one is left to wonder as to the origin of magnetic Mn sites in quasicrystals. There could be two possibilities.

First, does there exist another local symmetry which will leave the Mn moment intact. Our studies show that the p component at the Mn central site due to surrounding Al sites in MnAl clusters is the same as in pure Al clusters of the same size. This shows that those geometries which do not lead to Al p orbitals, which can mix with Mn d orbitals may stabilize the Mn moment. The second and more probable situation is that the Mn-Mn interactions are responsible for stabilizing magnetic sites. Indeed, the increase in the Mn moment with Mn concentration[8] suggests that this may be true. Indeed, our preliminary investigations support this latter possibility.

ACKNOWLEDGMENTS

We are grateful to J. van der Klink for helpful discussions and invaluable comments. We also thank J. Ph. Ansermet and J. Buttet for critical readings of the manuscript. This work was supported in part by the Swiss National Science Foundation under Grant No. 20-30272.90. One of us (S.N.K.) wants to thank Army Research Office (DAAL-03-89-K-0015) for financial support.

[1]D. Shechtman, I. Blech, D. Gratias, and J. W. Cahn, Phys. Rev. Lett. **53** 1951 (1984).

[2]W. W. Warren, Jr., H. S. Chen, and J. J. Hauser, Phys. Rev. B **32**, 7614 (1985); W. W. Warren, H. S. Chen, and G. P. Espinosa, *ibid.* **34**, 4902 (1986); Z. M. Stadnik, G. Stroink, H. Ma, and G. Williams, *ibid.* **39**, 9797 (1989); R. A. Dunlap, M. E. McHenry, V. Srinivas, D. Bahadur, and R. C. O'Handley, *ibid.* **39**, 4808 (1989).

[3]J. J. Hauser, H. S. Chen, and J. V. Waszczak, Phys. Rev. B **33**, 3577 (1986).

[4]*Introduction of Quasicrystals,* edited by M. V. Jaric (Academic, New York, 1988).

[5]P. Guyot and M. Audier, Philos. Mag. B **52**, L15 (1985); D. Levine and P. J. Steinhardt, Phys. Rev. Lett. **53**, 2477 (1984).

[6]A. L. Mackay, Acta Crystallogr. **15**, 916 (1962).

[7]M. Eibschutz, H. S. Chen, and J. J. Hauser, Phys. Rev. Lett. **56**, 169 (1986).

[8]J. Hauser, H. S. Chen, G. P. Espinosa, and J. V. Waszczak, Phys. Rev. B **34**, 4674 (1986).

[9]M. E. McHenry, D. D. Vvedensky, M. E. Eberhart, and R. C. O'Handley, Phys. Rev. B **37**, 10 887 (1988).

[10]D. Bagayoko, N. Brener, D. Kanhere, and J. Callaway, Phys. Rev. B **36**, 9263 (1987).

[11]G. B. Bachelet, D. R. Hammann, and M. Schluter, Phys. Rev. B **26**, 4199 (1982).

[12]D. M. Ceperley and B. J. Adler, Phys. Rev. Lett. **45**, 566 (1980).

[13]J. P. Perdew and A. Zunger, Phys. Rev. B **23**, 5048 (1981).

[14]W. Kohn and L. J. Sham, Phys. Rev. **140**, A1133 (1965).

[15]B. Roos, A. Veillard, and G. Vinot, Theor. Chim. Acta **20**, 1 (1971).

[16]A. J. H. Wachters, J. Chem. Phys. **52**, 1033 (1970).

[17]R. P. Messmer and S. H. Lamson, Chem. Phys. Lett. **90**, 31 (1982); K. Lee, J. Callaway, K. Kwong, R. Tang, and A. Ziegler, Phys. Rev. B **31**, 1796 (1985).

[18]M. Hamermesh, *Group Theory and its Applications to Physical*

Problems (Addison-Wesley, Reading, 1962); M. Tinkham, *Group Theory and Quantum Mechanics* (McGraw-Hill, New York, 1964); L. Jansen and M. Boon, *Theory of Finite Groups. Applications in Physics* (North-Holland, Amsterdam, 1967); T. Janssen, *Crystallographic Groups* (North-Holland, Amsterdam, 1973).

[19]B. I. Dunlap, Adv. Chem. Phys. **69**, 287 (1987).

[20]P. W. Atkins, M. S. Child, and C. S. G. Philips, *Tables for Group Theory* (Oxford University Press, New York, 1978).

[21]W. J. Hehre, L. Radom, P. v. R. Schleyer, and J. A. Pople, *Ab Initio Molecular Orbital Theory* (Wiley, New York, 1986).

[22]H. Sambe and R. H. Felton, J. Chem. Phys. **62**, 1122 (1975); B. I. Dunlap and J. W. D. Connolly, *ibid.* **71**, 4993 (1979).

[23]J. L. Martins, J. Buttet, and R. Car, Phys. Rev. B **31**, 1804 (1985); F. Reuse, S. N. Khanna, V. de Coulon, and J. Buttet, *ibid.* **41**, 11743 (1990).

[24]B. I. Dunlap, Phys. Rev. A **41**, 5691 (1990).